Osman Bahadır Özden ✉
Barış Gökçe
Abdullah Erdemir

https://doi.org/10.21278/TOF.494065224
ISSN 1333-1124
eISSN 1849-1391

A COMPARISON OF EFFECTS OF WELDING PARAMETERS IN T-JOINTS USING EXPERIMENTAL MODAL ANALYSIS AND FINITE ELEMENT MODELLING

Summary

Accurate determinations in the frequency domain are crucial in finite element analysis (FEA), particularly for ensuring the structural integrity of welded joints. FEA investigations are conducted on structures exposed to dynamic forcing conditions in various applications. When analysing dynamic conditions, employing modelling techniques in FEA is imperative to prevent failures occurring at natural frequencies. The natural frequency is influenced by welding parameters, which may vary based on different modelling approaches. This study compares the result of a modal analysis of 13 samples with the FEA results obtained through five distinct model methods of solid and shell model. Each sample in the experimental studies is prepared with different welding parameters, allowing for an examination of the effects of both welding and geometric parameters on the natural frequency. Additionally, the verification is performed by analysing the results of the samples scanned with a coordinate measuring machine (CMM) laser scanner. The obtained experimental data are compared with the finite element analyses and error rates are determined for each of the five model types. CMM model exhibits the highest accuracy with an error rate of 1.86%. Additionally, it is observed that solid model yields more precise results in instances where a CMM is unavailable, displaying an average error rate of 2.58%. As a result of the study, possible error rates in other model types in finite element analyses, either solid or shell model, are presented.

Key words: *experimental modal test; natural frequency; harmonic response analysis; finite element analysis; T-weld joints*

1. Introduction

Finite element analysis (FEA) serves a pivotal role in detecting structural damage across various applications. A critical parameter affecting structural damage is when the resonance frequency, often referred to as the natural frequency, is close to the forcing load frequency. FEA allows an analysis of structures that exist only geometrically, aiding in the production of results comparable to physically manifested structures. FEA modelling techniques chosen to provide results closest to the physical structure are growing in importance. In welded joints, FEA natural frequency results may change along with the material mechanical properties with high heat input [1]. Fatigue life is lower in welded joints compared to general structural steels. Low fatigue class (FAT) values become important for welded joints to be carefully examined in FEA. It is important to accurately evaluate natural frequencies, which have a significant impact on structural damage, especially in welded joints. In the FEA of vibrations, if the modal analyses are obtained incorrectly, the result of the vibration analysis are also incorrect. Therefore, in order to update FEA models correctly, the most accurate approach should be determined by comparing the FEA models with experimental studies in a real physical environment. With the increase in calculation techniques, predictions are made with FEA instead of experimental tests in many areas [2]. When performing tests for vibration-based models, there are response-based and modal-based methods. In response-based methods, evaluations are made by giving a frequency response function, but this method is not considered suitable for high-frequency structures. In another modal-based method, determinations can be made for high-frequency values along with natural frequency and mode shapes [3]. Across all disciplines in engineering, experimental methods are used to study how a system responds to a given input or forcing function. In experimental modal analysis (EMA) methods, natural frequency values are measured according to the techniques such as traditional contact-based impact hammer [4] or vibrator application [5], accelerometer response measurement, contactless speaker application [6], laser vibrometer [7], photogrammetry [8] and digital image correlation (DIC) response measurement [9]. Natural frequency results may vary depending on the choice of these methods and have been developed over time in the literature [10].

There are approaches to the fatigue life estimation of welded joints under dynamic stress conditions, according to the recommendations of the International Welding Institute. Effective notch stress approach examines the weld tip and weld root [11]. In this approach, for the FEA model, it is recommended to create a 1 mm radius at the weld tip and the fatigue class is selected as 225 MPa [12]. There are many models of welded joints, but their results may vary depending on experimental studies [13]. Due to the low fatigue life of welded joints, the selection of an FEA model for a modal analysis is important.

Since the 1990s, studies have continued to be carried out using the methodology and correlation development of accurate model in FEA, especially for dynamic forcing situations [14-16]. Rotondella et al. [2] made comparisons with modal tests and two different FEA models and determined the error rates. Recently, there have been many studies on FEA model verifications, comparing modal analysis and modal tests [17]. In a study, modal analysis results were compared according to six different FEA model techniques [18]. Abdullah et al. [19] updated the model to reduce the error rate by comparing FEA model and experimental studies on a vehicle in the automotive industry. Wen [20] validated FEA model with modal tests in two different applications. Abdullah et al. [21] compared the modal test data of the structure prepared with spot weld using four different FEA models and determined the error rates. While comparing the natural frequencies of welded joints in FEA, studies are carried out by applying many model techniques in complex structures or small samples [22-24]. Studies can be carried out not only to determine the dynamic characteristics but also for post-welding quality control purposes [25, 26]. Gharehbaghi et al. [27] examined the effects of residual stress on natural frequency experimentally and using FEA. Studies carried out to determine the natural frequency with modal tests are carried out in many areas such as aircraft wings, automotive industry, and offshore structures, where dynamic loads are involved, and are important for reducing structural errors [10, 28, 29]. Modal tests can also be performed on 3D printed parts [30]. Chen et al. [31] examined the results of a modal test and FEA of a wind turbine blade by scanning it with a 3D laser scanner. Gülbahçe and Çelik [32] performed modal tests on a steel plate by performing hammer roving. Additionally, there are numerous studies in the literature in which frequency spectra are examined using FEA, and structural integrity studies are conducted [33-37].

This paper presents effects of welding parameters using FEA and EMA of structures with welded joints. In this study, samples were prepared using metal active gas (MAG) welding according to 13 different welding parameters. Modal testing was carried out by connecting an accelerometer sensor to the prepared samples and hitting them with a hammer. The data were transferred to the frequency plane with the fast Fourier transform (FFT) and peak frequencies up to 6000 Hz, that is, natural frequencies, were determined. A solid model was prepared for FEA by laser scanning the samples with a CMM. Additionally, five different FEA model techniques were prepared and compared. Statistical data of each model were compared and the most accurate model technique was determined. Thus, the effects of welding parameters in each technique were determined.

2. Materials and methods

2.1 Samples and experimental setup

Ansys 2023 R2 software package was used for the numerical analysis. Spaceclaim and Solidworks computer aided design (CAD) software packages were also used for the numerical analysis and the production of samples. Thirteen different welding parameters were determined and samples were prepared. The samples were laser cut. The samples are made of S960QL ultra-high-strength steel, and a 1.2 mm filler wire was used for the welding seam. The filler wire material was Aristorod 89. Tensile tests were performed on these materials and the elasticity modulus was taken as 205 GPa. The mechanical properties of the filler wire and sample materials are close to each other [38]. The sample sizes are similar to sample sizes found in a study from the literature [39]. However, in order to see the effects of the geometric variables as well as the effects of the welding parameters, the workpiece and main material thickness, weld thickness, length and height values were changed in the preliminary design. Additionally, different samples were prepared to see the effects of multiple passes, preheating and interpass temperature values. All welds were made using robotic MAG welding. As presented in Table 1, different parameters were applied to each sample. All samples were prepared with a T-joint weld as shown in Fig. 1. In Fig. 1, a represents the weld throat thickness, l_1 represents the specimen width, t_1 represents the workpiece thickness, and l_2 represents the workpiece height. t_{pass} represents the interpass temperature and $t_{preheat}$ represents the preheat temperature. In the cases where $t_{preheat}$ was not applied, welding was performed at an ambient temperature of 22-25°C. A laser thermometer was used to measure the temperature. Voltage and current values were determined on a calibrated welding machine. All dimensions of the samples were checked after scanning with a CMM laser scanner.

Table 1 Samples for different parameters used in EMA and FEA

Sample	a /mm	Number of passes	Weld seam	t_1 /mm	l_2 /mm	l_1 /mm	$t_{preheat}$ /°C	t_{pass} /°C
SP-1	6.8-7.2	1	Convex	8	100	80	-	-
SP-2	6.8-7.2	1	Convex	5	100	80	-	-
SP-3	6.8-7.2	1	Convex	8	100	150	-	-
SP-4	2.9-3.2	1	Convex	8	100	80	-	-
SP-5	6.8-7.2	3	Convex	8	100	80	-	-
SP-6	6.8-7.2	1	Convex	8	100	80	100	-
SP-7	6.8-7.2	1	Convex	8	100	80	300	-
SP-8	6.8-7.2	1	Convex	15	100	80	-	-
SP-9	6.8-7.2	3	Convex	8	100	80	-	150
SP-10	6.8-7.2	1	Straight	8	100	80	-	-
SP-11	6.8-7.2	1	Concave	8	100	80	-	-
SP-12	6.8-7.2	4	Convex	8	100	80	-	150
SP-13	6.8-7.2	1	Convex	8	240	80	-	-

Voltage and current values were taken from the welding machine at different weld seams of the samples, as indicated in Table 2. Different welding parameters were used to obtain the weld throat thickness. As shown in Fig. 1 (a), a plate was placed at the beginning and end of the samples to get a stable weld seam. After the sample temperature reached room temperature, these plates were cut and the sample was obtained. Weld throat thickness was obtained in the samples between 6.8 and 7.2 mm and between 2.9 and 3.2 mm. These values were determined while examining the solid model after using the CMM laser scanner had been used. The reasons why the welding throat thicknesses are in this range are environmental conditions and fluctuations in the voltage and current values of the welding machine. Since the evaluations were also made on samples scanned with a CMM and this situation can also be encountered in real life, the FEA was evaluated by taking this into consideration. Three samples of each of the specified SP1-SP13 samples were prepared.

Table 2 Welding parameters of samples

Sample	Voltage /V	Current /A	Welding speed /(cm/dk)	Filler wire speed /(m/dk)
SP-1	27-32	280-300	25	12
SP-2	27-32	280-300	25	12
SP-3	27-32	280-300	25	12
SP-4	20-25	105-120	30	4
SP-5	27-32	280-300	25	12
SP-6	27-32	280-300	25	12
SP-7	27-32	280-300	25	12
SP-8	27-32	280-300	25	12
SP-9	25-30	250-270	55	12
SP-10	27-32	280-300	25	12
SP-11	27-32	280-300	25	12
SP-12	25-30	250-270	55	12
SP-13	27-32	280-300	25	12

In the EMA studies, ten points were determined on the sample prepared for hammer hitting. As shown in Fig. 1 (b), at points 1, 2, 3, 4, 5 and 6 in the -Y direction, at points 7 and 8 in the -Z direction, at point 9 in the -Z and +X direction, and at point 10 the hits were made with a hammer in the +X direction. At each point, at least five hits were made to avoid double hits, and the average of these hits was taken while taking the values with FFTs. If a double hit occurred during the hit, that is, if the hammer made more than one contact, that hit was cancelled. Thus, more stable data was obtained. In each sample, 55 hits were made from 11 hit directions. The total number of hammer hits for 13 samples was 715. By taking the average of the hits at each point, the peak frequency values in the results obtained with the FFT were determined as natural frequencies. Modes were also determined according to these natural frequency values, which vary in each sample. The accelerometer sensor was glued on the upper surface of the main material with an +30 mm adhesive. The sample was connected to the experimental setup, with an M20 10.9 bolt. The sample length is 150 mm and the main material thickness was 8 mm, but other geometric dimensions were changed. In addition, for the middle impact points, care was taken to ensure that they were not close to the accelerometer sensor, as stable data could not be obtained. Also, the impact was made from a central point half the height of the workpiece.

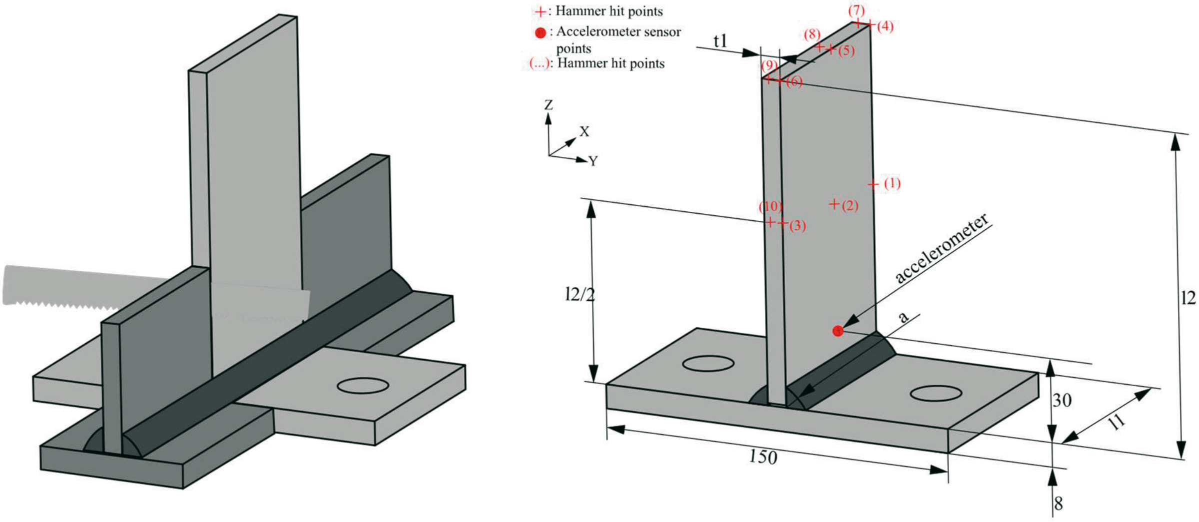

(a) (b)

Fig. 1 Sample geometric parameters, hammer impact points and accelerometer sensor points

Faro Quantums Max CMM was used for CMM laser scanning. Polyworks software was used and scanning settings were selected as Fine and geometries with 0.05 mm precision were obtained. The samples were scanned as shown in Fig. 2, and their bottom surfaces were scanned by rotating the sample and assembled in the Polyworks software. Error-free geometries were obtained by combining the bottom surface and other surfaces in the Polyworks software. Modal tests were carried out after the laser scanning process had been completed. In modal tests, Dewesoft Sirius was used as data acquisition (DAQ) hardware and DewesoftX software was also used for the interface. The data was filtered and time-dependent data was converted into frequency-dependent data with FFT. The accelerometer sensor sensitivity used was 0.01 m/s^2 and the hammer sensitivity was 0.1 N. Data were taken up to 6,000 Hz.

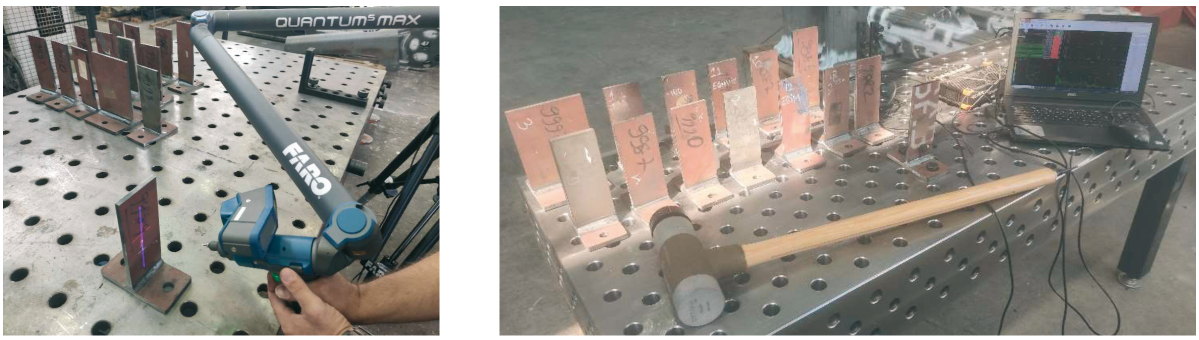

(a) (b)

Fig. 2 (a) CMM laser scanner setup, (b) Experimental setup for modal test

The modal parameter estimate was obtained based on a series of frequency response function (FRF) measurements. FRF defines the input-output relationship between two points on a structure as a function of frequency. In the performed modal test, the frequency response function (H(ω)) was obtained by dividing the Fourier transform of the output force (Y(ω)) by the Fourier transform X(ω) of the input response of the system [40]. The basic formula of the FRF is given below [41]:

$$H_{ij}(\omega) = \frac{Y_j(\omega)}{X_i(\omega)} \tag{1}$$

2.2 FEA model and theoretical background

Spaceclaim software was used to convert the scanned geometries into a solid model, using the Shrinkwrap command with an accuracy of 0.1 mm. The solid model is shown in Fig. 3. Despite the pre- and post-welding cleaning, welding slag appears in some areas. Since the tests were carried out with these slags, the CMM geometries were not changed. Compared to real geometries, quite perfect geometries were obtained and the mesh process was carried out in the Ansys Mechanical software. In the welding seam, the mesh size was entered as 0.1 mm, the element quality did not fall below 0.95, and the skewness did not exceed 0.15. The mesh size was determined as 0.1 mm after the mesh convergence process had been applied. After that, the natural frequencies above 0.1 decreased. Tetragonal mesh was used in the weld seam, and hexagonal mesh was used in other areas without weld seams.

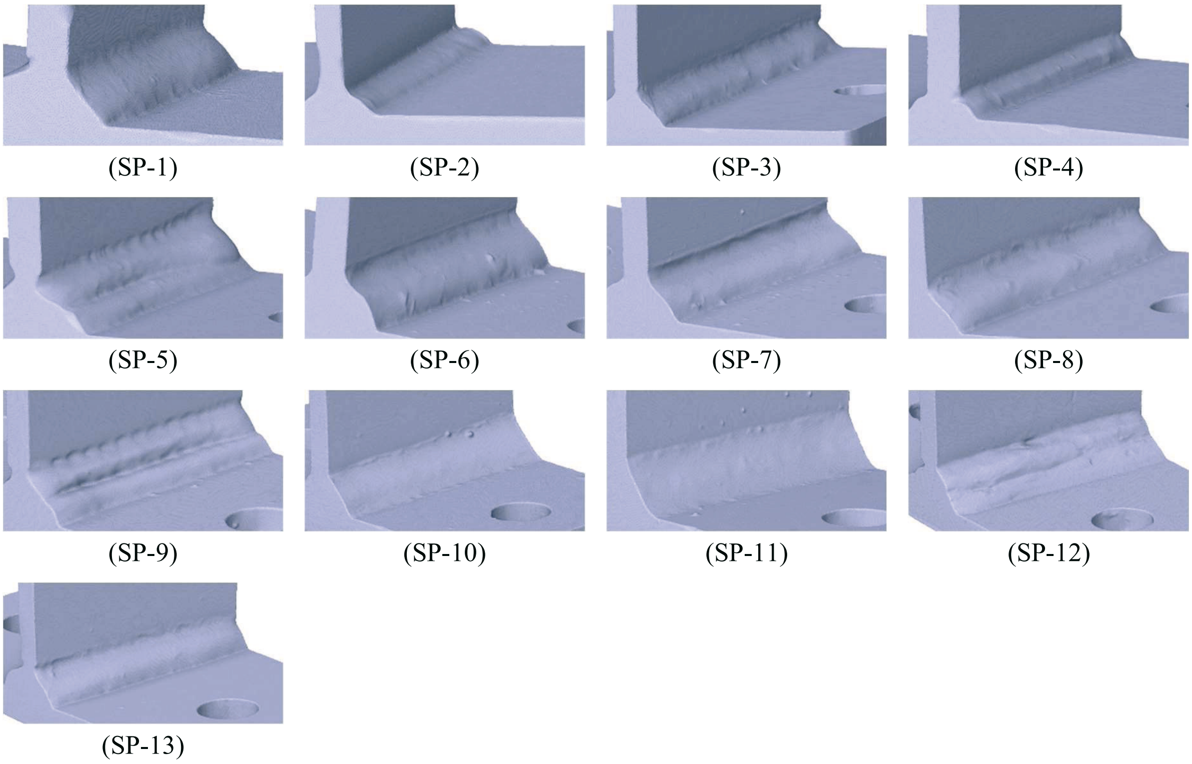

Fig. 3 FEA models obtained with CMM laser scanner

In the FEA, the models shown in Fig. 3 are defined as CMM models. Five models were applied: SHL-1, 2, 3 shell models and SLD-1, 2 solid models. In both model types, a contact definition called shared topology was made. In these models, the element quality did not exceed 0.95 and skewness did not exceed 0.15. Mesh convergence was applied in all models and the mesh size value was reduced until stable values were obtained. Hexagonal mesh was used in all SHL models. In SLD models, tetragonal mesh was used in the weld seam and hexagonal mesh was used in other regions. The reason for this is that there are too many hexagonal meshes in the solid models and there are defects in the weld seam. The model was defined in the FEA and connection holes were defined as boundary conditions, as shown in Fig. 4. Boundary conditions are defined as 0 mm in all axes. The workpiece is t_1, the main material is t_2, and the weld throat thickness is a. In the connection holes, the surface was created according to the surface area of the M20 bolt and fixed support was defined. Isotropic and homogeneous are assumed in the material definition. Since the study was carried out at room temperature and on the S960QL material, Young's modulus was defined as a constant of 205 GPa. This value was obtained as a result of the tensile test. Poisson's ratio was fixed and defined as 0.33 [42, 43].

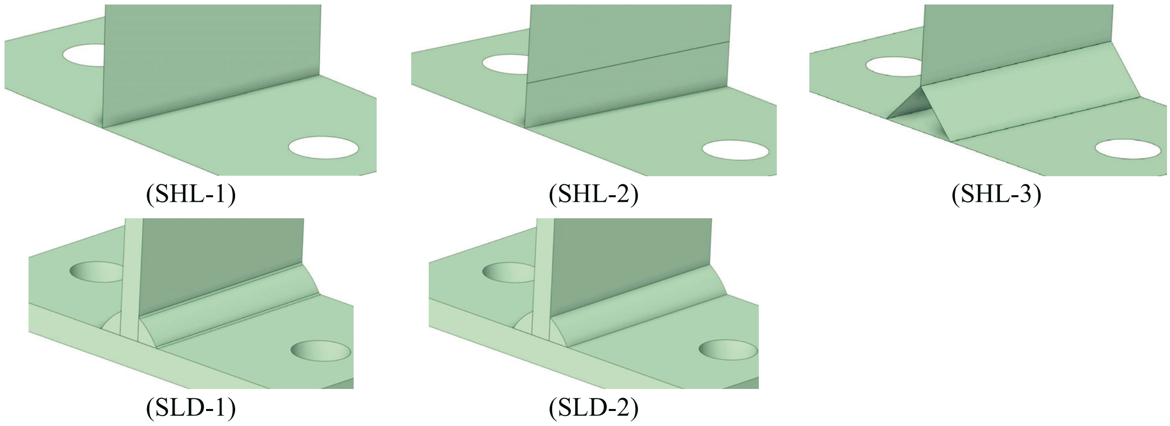

Fig. 4 FEA models used in comparison

The analyses were performed with linear material definitions according to the Euler-Bernoulli deformation approach and according to Hooke's law. The modal analyses were performed with these definitions and natural frequency values were determined. FEA can be used as a practical solution for the frequency responses of a complex structure [44]. In FEA, the general equation of motion called the governing equation, which is also used in multi-degree of freedom systems, is used. M is the mass, C is the dumping and K is the non-diagonal stiffness matrix. For the modal analysis, u and f are the vectors of Fourier transforms of displacement and force. The general motion equation used in the FEA [45] is as follows:

$$[\mathrm{M}]\{\ddot{\mathrm{u}}\}+[\mathrm{C}]\{\dot{\mathrm{u}}\}+[\mathrm{K}]\{\mathrm{u}\}=\{f(t)\}. \tag{2}$$

The natural frequency N degrees of freedom can be determined in an undampered and linear system by the following equation:

$$[\mathrm{M}]\{\ddot{\mathrm{u}}\}+[\mathrm{K}]\{\mathrm{u}\}=\{0\} \tag{3}$$

Assuming a harmonic response $x(t) = \mathrm{X}(\omega)\mathrm{e}^{i\omega t}$ with an angular frequency ω and response amplitude $\mathrm{X}(\omega)(\mathrm{N} \times 1)$, Eq. (3) can be rewritten as [46]:

$$\left[-\omega^2\mathrm{M}+\mathrm{K}\right]X(\omega)\mathrm{e}^{i\omega t}=0 \tag{4}$$

For natural frequency, Eq. Equation 3 is expressed as:

$$\left|-\omega^2\mathrm{M}+\mathrm{K}\right|=0 \tag{5}$$

Eq. 5. leads to quadratic equations with n joints. For this case, eigenvalue values were defined to be solved with an eigensystem:

$$\lambda_r=\omega_r{}^2 \tag{6}$$

where r is the mode number. The eigenvalue values are normalized eigenvector (Φ) values. The eigenvector values vary depending on the degree of freedom and the number of modes. Eigenvectors are also known as displacement mode shapes. In the harmonic response analysis, the coordinate system $\mathrm{X}(\omega)$ is converted into the modal coordinate system $q(\omega)$(Nx1) as follows:

$$X(\omega)=\Phi q(\omega) \tag{7}$$

While examining the frequency plane in a linear system, the following equation is used in the harmonic response analysis and the response of the system can be calculated as follows:

$$\left[-\omega^2\Phi^T M\Phi+i\omega\Phi^T C\Phi+\Phi^T K\Phi\right]q(\omega)=0 \tag{8}$$

FEA software consumes a very high disk capacity for a harmonic response analysis. If the frequency sensitivity value is set high, a low disk capacity will appear, but natural frequencies may not appear to peak. To prevent this problem, a script was prepared in the Python programming language. As seen in Fig. 5, this script saves the results to the solution database every 500 Hz and then deletes the analysis result so that it does not take up disk space. This process was applied for the harmonic response analysis of each of 13 samples. The number of samples in the loop is *j*, and *i* is defined as the frequency value. It continues and completes this cycle up to 6,000 Hz. This flowchart is defined by code in the journal script in Ansys Workbench. Analysis systems are opened as *j*-th systems, and within Ansys Mechanical, they define the frequency between *i* and *i*-500 and solve the analysis. In this way, results with a frequency sensitivity of 0.1 were obtained without taking up the space in the disk capacity.

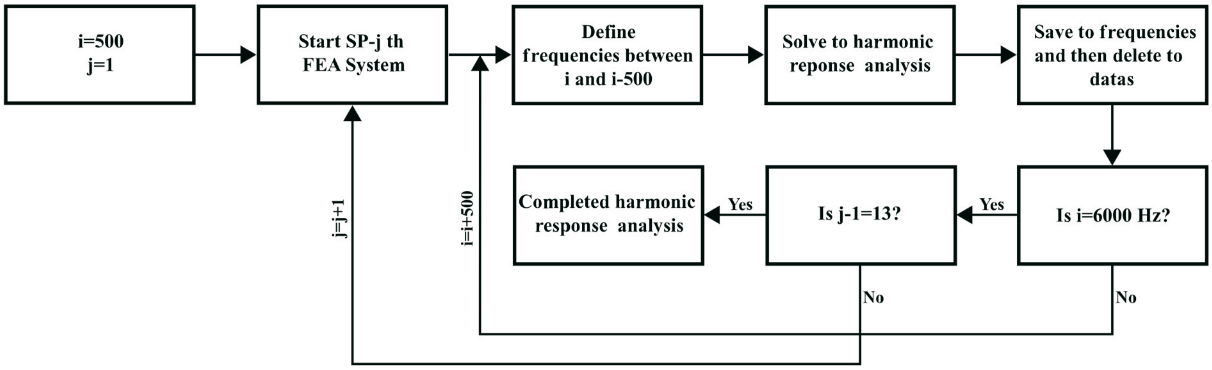

Fig. 5 Proposed flowchart for harmonic response analysis script

3. Results

In the study carried out with modal tests, time-dependent data was obtained using the data of the accelerometer sensor. The frequency plane was moved with the FFT and the peak frequencies were determined. After determining the natural frequencies, the analysis was performed for the same sample used in the FEA tests. As shown in Fig. 6, the frequency data obtained by the FFT of the experimentally obtained data were determined. In Fig. 6, only the results of the X, Y, and Z axes of the SP-1 sample are shown, and the results of the peak values of all samples are given in Table 3. Using Parseval's theorem, the power stability of the signal and power spectral density (PSD) values were obtained. The data obtained are the values obtained from the X, Y, and Z axes after removing noise and applying a filter to the data. Comparisons were made according to the results of this experimental study to determine the peak natural frequency values.

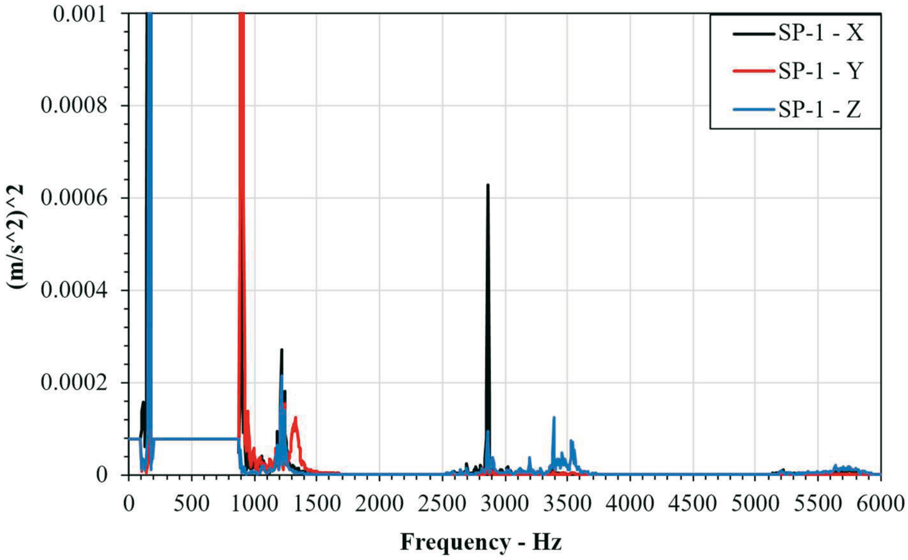

Fig. 6 Experimental modal test results obtained after FFT 0-6000 Hz for SP-1

Many model types prepared for the analysis models, and the model type called CMM are models created with a laser scanner. These models were used in the harmonic response analysis. A script was prepared for 13 samples, and in this script, the CMM samples were analysed through the loop. In the analysis of each sample, data were recorded every 500 Hz and analysis solutions were deleted. Thus, data with a sensitivity of 0.1 Hz was obtained, which does not take up disk space. Gravity was applied in the X, Y, and Z axis as loading condition. Consequently, mode shapes and frequency spectra in all axes were obtained. Fig. 7 shows the harmonic response analysis results for the X, Y, and Z axis on the SP-1 specimen for the CMM model. The natural frequency results of all other samples according to model techniques are given in Table 4. This script was also implemented for all other model types, and the natural frequencies of the model types are given in Table 3.

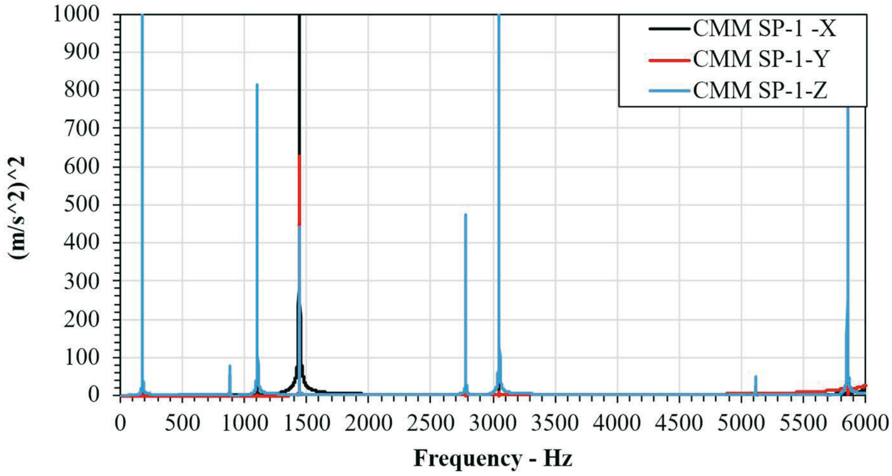

Fig. 7 Harmonic response analysis for CMM models

As FEA model types, five models called SLD and SHL, along with solid and shell models, were prepared. Modal analysis was performed in each model. As a result of this analysis, the natural frequency of each sample was determined. The natural frequency values obtained from the EMA are shown in Table 3. In the finite element analyses, numerical analysis was carried out for up to seven modes and a maximum natural frequency of up to 6000 Hz was determined.

Table 3 Natural frequency results of EMA of samples

	Mod 1 /Hz	**Mod 2** /Hz	**Mod 3** /Hz	**Mod 4** /Hz	**Mod 5** /Hz	**Mod 6** /Hz	**Mod 7** /Hz
SP 1 EMA	169.92	890.63	1,130.86	1,417.97	2,859.38	3,111.33	5,203.13
SP 2 EMA	111.33	556.64	673.83	1,400.39	1,769.53	1,863.28	3,228.52
SP 3 EMA	175.78	521.48	1,048.83	1,916.02	2,197.27	2,273.44	3,064.45
SP 4 EMA	169.92	867.19	1,054.69	1,429.69	2,748.05	2,912.11	4,992.19
SP 5 EMA	181.64	890.63	1,083.98	1,429.69	2,876.95	3,152.34	5,326.17
SP 6 EMA	175.78	884.77	1,066.41	1,517.58	2,900.39	3,146.48	5,296.88
SP 7 EMA	175.74	884.71	1,065.42	1,517.58	2,724.61	2,835.94	4,013.67
SP 8 EMA	304.69	1,417.97	1,564.45	1,863.28	4,687.50	4,910.20	
SP 9 EMA	181.64	902.34	1,113.28	1,511.72	2,906.11	3,240.23	5,320.31
SP 10 EMA	175.78	878.91	1,078.13	1,450.10	2,812.50	3,017.58	5,261.76
SP 11 EMA	181.64	884.77	1,107.42	1,435.55	2,894.53	3,011.72	5,390.63
SP 12 EMA	181.62	908.20	1,106.41	1,488.21	2,830.07	3,228.57	5,367.20
SP 13 EMA	123.05	685.55	767.58	1,019.53	2,156.25	2,255.86	3,966.80

In Table 4, the data obtained from the modal analysis are given: only up to 6 modes were taken in SP-9, and the 7th mode was not evaluated because it exceeded the value of 6,000 Hz.

The maximum frequency in the 7th mode is 5,417.60 Hz and was found in the SP-10 sample. The 8th mode frequencies exceeded 6,000 Hz in all samples, and the first 7 modes were evaluated to compare them with the experimental studies. Different natural frequency values were determined in each sample and in each mode. It can be seen that there are differences in samples SP-2, 3, 8, and 13, where the workpiece and the main material thicknesses and heights vary, compared to other samples due to their effect on the stiffness matrix. These differences affected each mode. In other samples, less differences in the natural frequencies were detected due to the effect of preheating and interpass temperatures, and different results were detected in each mode. It was observed that each parameter determined during the preparation of the samples has an effect.

Table 4 Natural frequency results of EMA of samples

	Mod 1 /Hz	**Mod 2** /Hz	**Mod 3** /Hz	**Mod 4** /Hz	**Mod 5** /Hz	**Mod 6** /Hz	**Mod 7** /Hz
SP 1 CMM	169.92	890.63	1,130.86	1,417.97	2,859.38	3,111.33	5,203.13
SP 1 SLD-1	173.84	879.80	1,103.60	1,442.10	2,781.70	3,050.20	5,117.40
SP 1 SLD-2	175.54	864.81	1,087.70	1,457.20	2,745.60	3,015.40	5,049.70
SP 1 SHL-1	175.67	867.40	1,089.00	1,455.60	2,755.20	3,021.40	5,071.50
SP 1 SHL-2	166.24	848.76	1,035.90	1,485.70	2,706.40	2,906.70	5,028.50
SP 1 SHL-3	185.97	903.32	1,157.60	1,561.50	2,894.20	3,245.00	5,417.60
SP 2 CMM	187.27	901.95	1,160.80	1,571.40	2,888.50	3,235.60	5,387.10
SP 2 SLD-1	111.33	556.64	673.83	1,400.39	1,769.53	1,863.28	3,228.52
SP 2 SLD-2	105.39	542.93	662.59	1,393.30	1,740.90	1,859.40	3,219.40
SP 2 SHL-1	111.55	555.52	694.10	1,483.70	1,771.60	1,939.70	3,284.60
SP 2 SHL-2	111.26	554.82	692.41	1,481.60	1,769.20	1,935.30	3,279.90
SP 2 SHL-3	104.13	539.50	651.98	1,485.70	1,730.20	1,847.30	3,242.80
SP 3 CMM	119.10	581.65	745.94	1,585.20	1,878.10	2,115.40	3,558.40
SP 3 SLD-1	118.91	579.37	742.98	1,595.70	1,869.60	2,100.40	3,534.10
SP 3 SLD-2	175.78	521.48	1,048.83	1,916.02	2,197.27	2,273.44	3,064.45
SP 3 SHL-1	176.93	522.55	1,068.62	1,815.30	2,129.50	2,271.70	3,101.90
SP 3 SHL-2	177.79	524.07	1,094.50	1,797.80	2,110.00	2,270.50	3,067.70
SP 3 SHL-3	177.47	523.56	1,092.70	1,795.90	2,109.60	2,267.60	3,063.20
SP 4 CMM	167.85	507.74	1,037.30	1,737.40	2,102.80	2,284.60	2,929.00
SP 4 SLD-1	187.85	543.04	1,157.30	1,873.70	2,133.90	2,387.70	3,254.00
SP 4 SLD-2	189.17	543.86	1,160.90	1,873.50	2,133.00	2,396.50	3,248.40
SP 4 SHL-1	169.92	867.19	1,054.69	1,429.69	2,748.05	2,912.11	4,992.19
SP 4 SHL-2	167.57	857.21	1,043.80	1,409.10	2,732.80	2,898.90	4,925.90
SP 4 SHL-3	167.82	850.94	1,050.80	1,401.50	2,726.60	2,944.70	4,991.10
SP 5 CMM	171.50	855.96	1,063.40	1,435.30	2,716.50	2,951.90	4,993.20
SP 5 SLD-1	166.25	846.21	1,034.10	1,471.80	2,686.80	2,888.90	4,945.20
SP 5 SLD-2	171.54	861.48	1,067.10	1,494.30	2,738.50	2,980.30	5,051.70
SP 5 SHL-1	180.59	881.86	1,116.10	1,533.40	2,817.30	3,103.10	5,235.30
SP 5 SHL-2	181.64	890.63	1,083.98	1,429.69	2,876.95	3,152.34	5,326.17
SP 5 SHL-3	180.36	885.24	1,121.80	1,449.10	2,803.10	3,105.60	5,183.50
SP 6 CMM	175.54	864.81	1,087.70	1,457.20	2,745.60	3,015.40	5,049.70
SP 6 SLD-1	175.67	867.40	1,089.00	1,455.60	2,755.20	3,021.40	5,071.50
SP 6 SLD-2	166.24	848.76	1,035.90	1,485.70	2,706.40	2,906.70	5,028.50
SP 6 SHL-1	185.97	903.32	1,157.60	1,561.50	2,894.20	3,245.00	5,417.60
SP 6 SHL-2	187.27	901.95	1,160.80	1,571.40	2,888.50	3,235.60	5,387.10
SP 6 SHL-3	175.78	884.77	1,066.41	1,517.58	2,900.39	3,146.48	5,296.88
SP 7 CMM	178.75	883.60	1,114.20	1,444.30	2,812.70	3,086.90	5,165.50
SP 7 SLD-1	175.54	864.81	1,087.70	1,457.20	2,745.60	3,015.40	5,049.70
SP 7 SLD-2	175.67	867.40	1,089.00	1,455.60	2,755.20	3,021.40	5,071.50

	Mod 1 /Hz	**Mod 2** /Hz	**Mod 3** /Hz	**Mod 4** /Hz	**Mod 5** /Hz	**Mod 6** /Hz	**Mod 7** /Hz
SP 7 SHL-1	166.24	848.76	1,035.90	1,485.70	2,706.40	2,906.70	5,028.50
SP 7 SHL-2	185.97	903.32	1,157.60	1,561.50	2,894.20	3,245.00	5,417.60
SP 7 SHL-3	187.27	901.95	1,160.80	1,571.40	2,888.50	3,235.60	5,387.10
SP 8 CMM	175.74	884.71	1,065.42	1,517.58	2,724.61	2,835.94	4,013.67
SP 8 SLD-1	175.38	867.11	1,088.10	1,430.40	2,750.20	3,017.90	4,068.60
SP 8 SLD-2	175.54	864.81	1,087.70	1,457.20	2,745.60	3,015.40	4,049.70
SP 8 SHL-1	175.67	867.40	1,089.00	1,455.60	2,755.20	3,021.40	4,071.50
SP 8 SHL-2	166.24	848.76	1,035.90	1,485.70	2,706.40	2,906.70	4,028.50
SP 8 SHL-3	185.97	903.32	1,157.60	1,561.50	2,894.20	3,245.00	4,417.60
SP 9 CMM	187.27	901.95	1,160.80	1,571.40	2,888.50	3,235.60	4,387.10
SP 9 SLD-1	304.69	1,417.97	1,564.45	1,863.28	4,687.50	4,910.20	-
SP 9 SLD-2	312.74	1,413.30	1,492.70	1,911.40	4,683.40	5,166.50	-
SP 9 SHL-1	319.31	1,425.00	1,519.00	1,947.10	4,755.80	5,253.10	-
SP 9 SHL-2	318.65	1,423.90	1,517.70	1,943.60	4,751.70	5,245.00	-
SP 9 SHL-3	309.87	1,485.90	1,507.90	1,895.80	4,734.10	5,163.30	-
SP 10 CMM	328.43	1,534.70	1,563.30	2,010.90	4,918.80	5,479.10	-
SP 10 SLD-1	341.92	1,548.20	1,579.70	2,070.40	4,965.40	5,568.60	-
SP 10 SLD-2	181.64	902.34	1,113.28	1,511.72	2,906.11	3,240.23	5,320.31
SP 10 SHL-1	181.28	886.83	1,122.80	1,455.80	2,807.10	3,102.40	5,168.80
SP 10 SHL-2	175.54	864.81	1,087.70	1,457.20	2,745.60	3,015.40	5,049.70
SP 10 SHL-3	175.67	867.40	1,089.00	1,455.60	2,755.20	3,021.40	5,071.50
SP 11 CMM	166.24	848.76	1,035.90	1,485.70	2,706.40	2,906.70	5,028.50
SP 11 SLD-1	185.97	903.32	1,157.60	1,561.50	2,894.20	3,245.00	5,417.60
SP 11 SLD-2	187.27	901.95	1,160.80	1,571.40	2,888.50	3,235.60	5,387.10
SP 11 SHL-1	175.78	878.91	1,078.13	1,450.10	2,812.50	3,017.58	5,261.76
SP 11 SHL-2	178.37	877.70	1,115.30	1,430.40	2,815.40	3,099.90	5,276.40
SP 11 SHL-3	175.54	864.81	1,087.70	1,457.20	2,745.60	3,015.40	5,049.70
SP 12 CMM	175.67	867.40	1,089.00	1,455.60	2,755.20	3,021.40	5,071.50
SP 12 SLD-1	166.24	848.76	1,035.90	1,485.70	2,706.40	2,906.70	5,028.50
SP 12 SLD-2	185.97	903.32	1,157.60	1,561.50	2,894.20	3,245.00	5,417.60
SP 12 SHL-1	187.27	901.95	1,160.80	1,571.40	2,888.50	3,235.60	5,387.10
SP 12 SHL-2	181.64	884.77	1,107.42	1,435.55	2,894.53	3,011.72	5,390.63
SP 12 SHL-3	182.11	889.96	1,131.20	1,453.30	2,830.40	3,128.50	5,206.50
SP 13 CMM	176.38	880.13	1,120.20	1,446.20	2,802.50	3,050.40	5,355.60
SP 13 SLD-1	179.47	876.94	1,111.40	1,473.70	2,787.00	3,080.40	5,134.60
SP 13 SLD-2	166.24	848.76	1,035.90	1,485.70	2,706.40	2,906.70	5,028.50
SP 13 SHL-1	185.97	903.32	1,157.60	1,561.50	2,894.20	3,245.00	5,417.60
SP 13 SHL-2	187.27	901.95	1,160.80	1,571.40	2,888.50	3,235.60	5,387.10
SP 13 SHL-3	181.62	908.20	1,106.41	1,488.21	2,830.07	3,228.57	5,367.20

In the modal analysis, mode shapes were also determined. The mode shapes are used only to examine the directional effects of different parameters and to indicate them in shape. The mode shapes of the CMM models are shown in Fig. 8. When examining in the frequency plane, natural frequency evaluations affect the results of the analysis types such as the fatigue analysis. PSD values may change depending on the damping ratio, but their frequencies remain constant. Therefore, the mode shapes were examined only to see the directional effects rather than to make a comparison with the modal assurance criteria.

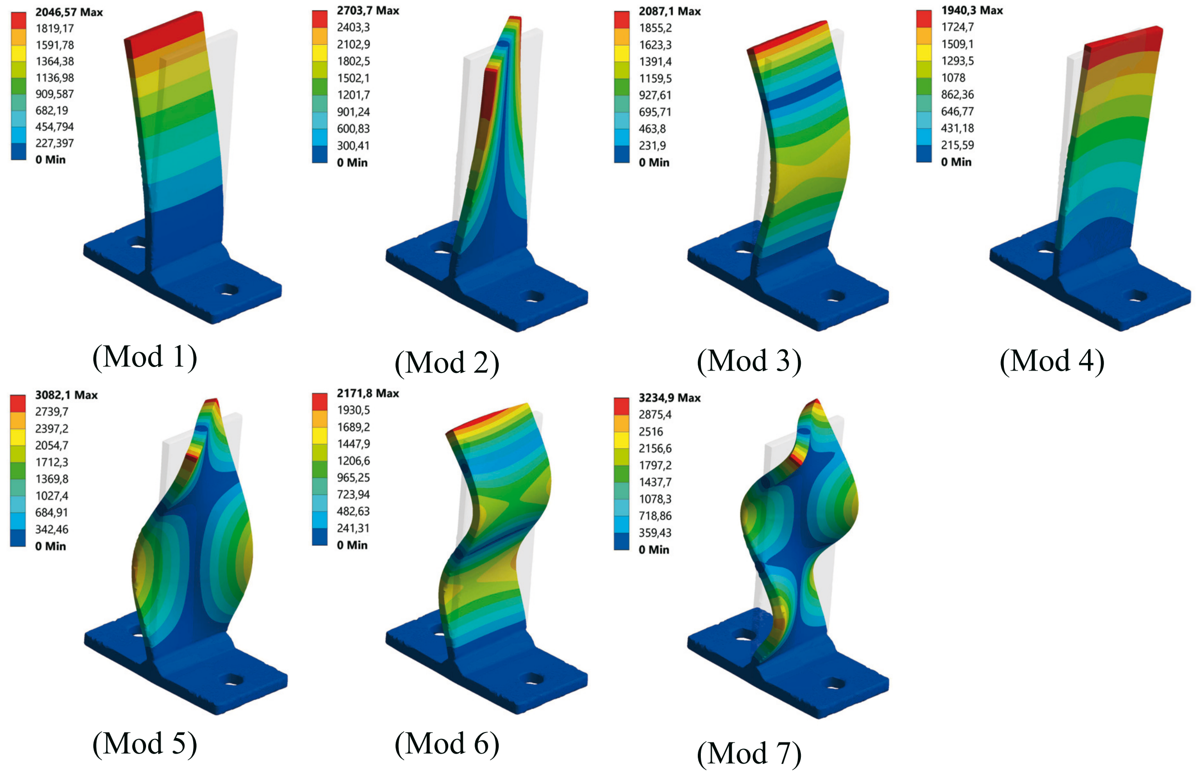

Fig. 8 SP-1 CMM mode shapes resulting from analysis

As seen in Fig. 9, the experimental studies of each sample were compared with the CMM, SLD and SHL model and the error rates were determined only for the SP-1 sample. The statistical results of other samples are given in Table 5. It can be seen that there are different error rates in each sample in each model type. Higher error rates were detected in SHL-2 and SHL-3 model types compared to other model types. It is observed that the error rates are in a wider range, especially in the 4th mode, which exhibits the direction of progress. In the 2nd mode, the error rate and width ranges are less. In addition, the error rate ranges in the 5th mode are quite low and have a similar mode shape as the 2nd mode. When the mode shapes are examined, very accurate results are determined for the 2nd and 5th modes, which are torsion modes.

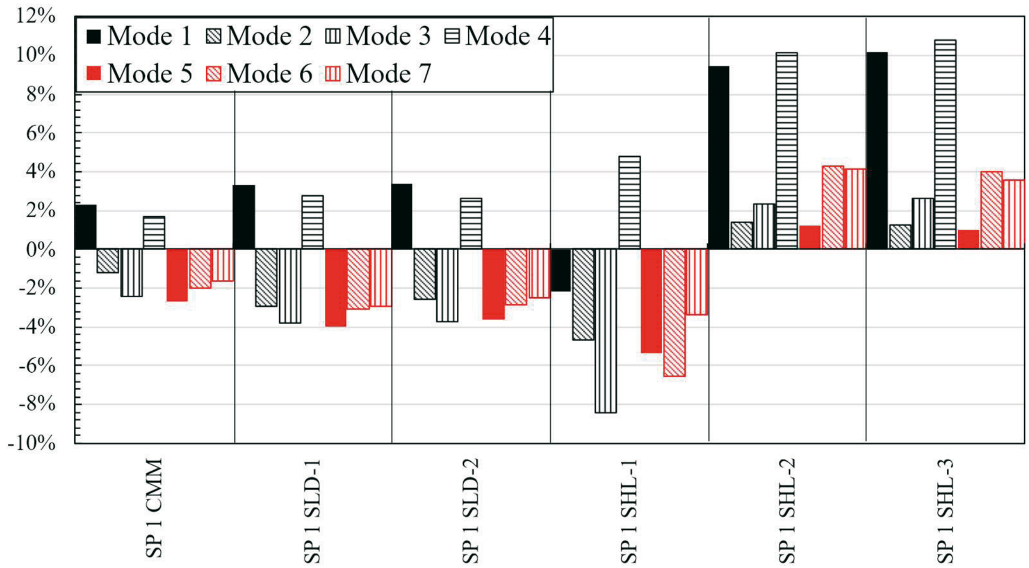

Fig. 9 Results of natural frequency error rates of SP-1 FEA model

The statistical results determined as a result of comparisons of natural frequencies are given in Table 5. Each model type was based on the results of all samples. SLD-1 and SHL-1 models are the model types with the lowest error rates according to the averages determined in the analysis of all samples. However, based on absolute values, the SHL-1 model gives results with a higher error rate than the SLD models. The SLD model, which is a solid model, has lower absolute average values than the SHL model, which are shell model types. For the SHL model types, the SHL-1 model error rates gave the lowest results.

Table 5 Statistical results obtained by experimental and FEA comparisons

	Average error rate	Absolute average error rate	Standard deviation of average error rates	RMSE
Modal Test	0.00%	0.00%	0.00%	0.00
CMM	-0.39%	1.86%	1.19%	6.25
SLD-1	-0.88%	2.58%	10.62%	9.89
SLD-2	-0.74%	2.56%	8.63%	12.93
SHL-1	-2.90%	4.17%	7.32%	15.09
SHL-2	4.25%	4.49%	10.56%	147.79
SHL-3	4.75%	5.05%	10.43%	163.75

In some previous studies, welded joints were compared on the frequency plane in FEA and experimental studies and examined according to only one parameter [26]. In some studies, complex structures were examined [28]. There are also studies examining the effect of heat input on the natural frequency for only a single parameter in butt welding [25]. There are comparisons involving shell and solid model for butt welding, but CMM model was not performed, and solid model gave more accurate results [18]. In this study, the effects of 13 welds and geometric parameters for T-joints were examined and compared with FEA. Results with the lowest error rate were obtained with a CMM model. The solid model results have been found to have lower error rates than shell model results. The solution time of solid models is longer and the model preparation effort is higher, and if shell model is preferred, it was observed that the SHL-1 model has an average error rate of 4.17% in the frequency plane. However, the effects of the welding parameters should be taken into account. If one of the 13 parameters is chosen, the error rates obtained in this study should be taken into consideration. As a result of this study, it is suggested that the preferred model type may cause error rates in 13 parameters and should be evaluated accordingly.

4. CONCLUSION

In this study, a comprehensive analysis was undertaken to assess five distinct model types of welded joints using FEA, juxtaposed against models obtained through laser scanning and modal test studies. Across 13 welding and geometric parameters, an in-depth examination was conducted to understand the nuanced effects of these parameters and to scrutinize the associated error rates. The CMM model emerged as the standout performer, showcasing the lowest absolute average error rate at an impressive 1.86%. In instances where laser scanning was impractical, the SLD-1 model proved to be the most optimal alternative, exhibiting the lowest average error rate of 2.58%. While SLD models demand bigger effort compared to SHL models, the SHL-1 model is recommended for the shell model due to its lower average error rate of 4.17%. As a result of the experimental and numerical analyses carried out for the determination of natural frequencies, the following conclusions can be reached:

1. As a result of the experimental studies, the effects of 13 different parameters on the natural frequency in the T-joint weld were revealed. The error rates of all parameters were determined.

2. Natural frequency results and error rates were obtained according to six different model techniques. It was determined that the CMM model was the most accurate of all model types and this model technique is recommended.
3. For the harmonic response analysis, the recommendation is to employ a script algorithm embedded within FEA software. This strategic suggestion not only mitigates potential challenges related to disk insufficiency in high-capacity scenarios but also ensures a precise determination of frequency values.
4. In the cases where it is not possible to create a CMM model technique, other model techniques, divided into solid and shell models, can be preferred. In the case when these are preferred, the effects of the parameters, the examined mode shape and the model technique error rates should be taken into account.

Acknowledgments

The authors gratefully acknowledge the support of MPG Machinery Production Group Inc. Co. This study was carried out within the scope of a doctoral thesis.

REFERENCES

[1] Sharma, A., A.K. Bagha, D.K. Shukla, and S. Bahl, Finite element model updating of metallic and composite structures--A state of the art review. AIMS Materials Science, 2021, 8(3). https://doi.org/10.3934/matersci.2021025

[2] Rotondella, V., A. Merulla, A. Baldini, and S. Mantovani, Dynamic modal correlation of an automotive rear subframe, with particular reference to the modelling of welded joints. Advances in Acoustics and Vibration, 2017, 2017. https://doi.org/10.1155/2017/8572674

[3] Esfandiari, A., F. Bakhtiari-Nejad, M. Sanayei, and A. Rahai, Structural finite element model updating using transfer function data. Computers & structures, 2010, 88(1-2): p. 54-64. https://doi.org/10.1016/j.compstruc.2009.09.004

[4] Warren, C., C. Niezrecki, P. Avitabile, and P. Pingle, Comparison of FRF measurements and mode shapes determined using optically image based, laser, and accelerometer measurements. Mechanical Systems and Signal Processing, 2011, 25(6): p. 2191-2202. https://doi.org/10.1016/j.ymssp.2011.01.018

[5] Kalybek, M., M. Bocian, W. Pakos, J. Grosel, and N. Nikitas, Performance of camera-based vibration monitoring systems in input-output modal identification using shaker excitation. Remote Sensing, 2021, 13(17): p. 3471. https://doi.org/10.3390/rs13173471

[6] Hu, Y., W. Guo, W. Zhu, and Y. Xu, Local damage detection of membranes based on Bayesian operational modal analysis and three-dimensional digital image correlation. Mechanical Systems and Signal Processing, 2019, 131: p. 633-648. https://doi.org/10.1016/j.ymssp.2019.04.051

[7] Xu, Y., D.-M. Chen, and W. Zhu, Damage identification of beam structures using free response shapes obtained by use of a continuously scanning laser Doppler vibrometer system. Mechanical Systems and Signal Processing, 2017, 92: p. 226-247. https://doi.org/10.1016/j.ymssp.2016.12.042

[8] Gwashavanhu, B., A.J. Oberholster, and P.S. Heyns, Rotating blade vibration analysis using photogrammetry and tracking laser Doppler vibrometry. Mechanical Systems and Signal Processing, 2016, 76: p. 174-186. https://doi.org/10.1016/j.ymssp.2016.02.019

[9] Perić, M., Z. Tonković, A. Rodić, M. Surjak, et al., Numerical analysis and experimental investigation of welding residual stresses and distortions in a T-joint fillet weld. Materials & Design, 2014, 53: p. 1052-1063. https://doi.org/10.1016/j.matdes.2013.08.011

[10] Will, D.T. and W. Zhu, Experimental Modal Analysis and Operational Deflection Shape Analysis of a Cantilever Plate in a Wind Tunnel with Finite Element Model Verification. Experimental Techniques, 2023: p. 1-20. https://doi.org/10.1007/s40799-023-00682-w

[11] Hobbacher, A., Recommendations for fatigue design of welded joints and components. Vol. 47. 2016: Springer. https://doi.org/10.1007/978-3-319-23757-2

[12] Fricke, W., IIW recommendations for the fatigue assessment of welded structures by notch stress analysis: IIW-2006-09. 2012: Woodhead Publishing. https://doi.org/10.1533/9780857098566

[13] Büyükbayram, C., B. Koç, G. Tekin, and B. Salihoğlu, Fatigue strength evaluation approach of welded joints for more reliable and lighter military ground vehicles. Procedia Engineering, 2015, 133: p. 485-500. https://doi.org/10.1016/j.proeng.2015.12.619

[14] Ren, W.-X. and H.-B. Chen, Finite element model updating in structural dynamics by using the response surface method. Engineering structures, 2010, 32(8): p. 2455-2465. https://doi.org/10.1016/j.engstruct.2010.04.019

[15] Friswell, M. and J.E. Mottershead, Finite element model updating in structural dynamics. Vol. 38. 1995: Springer Science & Business Media. https://doi.org/10.1007/978-94-015-8508-8

[16] Baker, M. Review of test/analysis correlation methods and criteria for validation of finite element models for dynamic analysis. in 10th International Modal Analysis Conference. 1992.

[17] Ereiz, S., I. Duvnjak, and J.F. Jiménez-Alonso. Review of finite element model updating methods for structural applications. in Structures. 2022. Elsevier. https://doi.org/10.1016/j.istruc.2022.05.041

[18] de Arruda, M.V., E.O. Correa, and V.B.d.P. Macanhan, Optimization of FEM models for welding residual stress analysis using the modal method. Welding in the World, 2023, 67(10): p. 2361-2372. https://doi.org/10.1007/s40194-023-01570-y

[19] Abdullah, N., M. Fouzi, and M.M. Sani, Computational modal analysis on finite element model of body-in-white structure and its correlation with experimental data. International Journal of Automotive and Mechanical Engineering, 2020, 17(2): p. 7915-7926

[20] Wen, J.H., FEA Modeling verification and validation: correlating model with test data by optimization analysis. 2007. https://doi.org/10.4271/2007-01-1745

[21] Abdullah, N., M. Asri, and M.S.M. Sani, Strategies of Finite Element Modeling for Spot Welded Joints and its Modal Correlation with Experimental Data. International Journal of Automotive and Mechanical Engineering, 2022, 19(1): p. 9543-9550. https://doi.org/10.15282/ijame.19.1.2022.17.0736

[22] Fouzi, M., K. Jelani, N. Nazri, and M.S.M. Sani, Finite element modelling and updating of welded thin-walled beam. International Journal of Automotive and Mechanical Engineering, 2018, 15(4): p. 5874-5889. https://doi.org/10.15282/ijame.15.4.2018.12.0449

[23] Fouzi, M., M. Sani, and Y. Muchlis. Finite Element Modelling and updating of welded joint for dynamic study of exhaust structure. in IOP Conference Series: Materials Science and Engineering. 2019. IOP Publishing. https://doi.org/10.1088/1757-899X/469/1/012099

[24] Husain, N.A., H.H. Khodaparast, A. Snaylam, S. James, et al. Modal testing and finite element model updating of laser spot welds. in Journal of Physics: Conference Series. 2009. IOP Publishing. https://doi.org/10.1088/1742-6596/181/1/012024

[25] Rajaei, M., S.H. Elahi, and M. Mashhadgarme, A novel method for quality control of post weld heat treatment process using modal parameters. NDT & E International, 2020, 111: p. 102216. https://doi.org/10.1016/j.ndteint.2020.102216

[26] Shrivastava, K., K. Vijayan, and V. Arora, Experimental identification of dynamic characteristics of welded stiffened structures based on model updating. Thin-Walled Structures, 2023, 184: p. 110485. https://doi.org/10.1016/j.tws.2022.110485

[27] Gharehbaghi, H., S. Hosseini, and R. Hosseini, Investigation of the Effect of Welding Residual Stress on Natural Frequencies, Experimental and Numerical Study. Iranian Journal of Science and Technology, Transactions of Mechanical Engineering, 2023, 47(4): p. 1777-1785. https://doi.org/10.1007/s40997-022-00588-9

[28] Andika, M.G., M.A. Moelyadi, R.A. Sasongko, and B.K. Hadi, Pretest Planning Approach for Optimal Modal Testing on High Aspect Ratio Wing Structure. Iranian Journal of Science and Technology, Transactions of Mechanical Engineering, 2023, 47(3): p. 1109-1120. https://doi.org/10.1007/s40997-022-00564-3

[29] Mirza, W.W.I., M.A. Rani, M. Yunus, B. Athikary, and M. Sani, Correlating finite element model of a car spot-welded front-end module in the light of modal testing data. International Journal of Automotive and Mechanical Engineering, 2020, 17(2): p. 7974-7984. https://doi.org/10.15282/ijame.17.2.2020.16.0597

[30] Foroozanfar, A., M. Afridi, K. Fayazbakhsh, and S. Hashemi, Experimental and Computational Analysis of Elastic Modulus of 3D Printed Parts Using Impulse Excitation Technique (IET). Experimental Techniques, 2023, 47(4): p. 787-795. https://doi.org/10.1007/s40799-022-00592-3

[31] Chen, Y., A. Escalera Mendoza, and D. Griffith, Experimental dynamic characterization of both surfaces of structures using 3d scanning laser doppler vibrometer. Experimental Techniques, 2023, 47(5): p. 989-1006. https://doi.org/10.1007/s40799-022-00604-2

[32] Gülbahçe, E. and M. Çelik, Experimental modal analysis for the plate structures with roving inertial shaker method approach. Journal of Low Frequency Noise, Vibration and Active Control, 2022, 41(1): p. 27-40. https://doi.org/10.1177/14613484211039323

[33] Aydın, K., A. Akgün, Ç. Yavaş, A. Gök, and U. Şeker, Experimental and numerical study of cutting force performance of wave form end mills on Gray Cast Iron. Arabian Journal for Science and Engineering, 2021, 46: p. 12299-12307. https://doi.org/10.1007/s13369-021-05816-z

[34] Gök, A., H. Demirci, and K. Gök, Determination of experimental, analytical, and numerical values of tool deflection at ball end milling of inclined surfaces. Proceedings of the institution of mechanical engineers, part e: journal of process mechanical engineering, 2016, 230(2): p. 111-119. https://doi.org/10.1177/0954408914540633

[35] Serkan Caska, M.E.D., Kadir Gok, Levent Urtekin and Arif Gok, Obtaining Vibration Models of a Lattice Structured Cantilever Beam Constructed with Different Types of Materials. Annals of Civil Engineering and Management, 2024, 1(1): p. 1-7. https://doi.org/10.33140/ACEM.01.01.01

[36] Gok, K., G. Karagoz, and A. Gok, Vibration Damper Design and Additive Manufacturing for Unmanned Aerial Vehicles. Journal of Mechanical Materials and Mechanics Research| Volume, 2023, 6(02). https://doi.org/10.30564/jmmmr.v6i2.5711

[37] Gok, K., E. Turkes, Ö. Karakas, and A. Gok, Analyzing the Effects of Tool Holder Stiffness on Chatter Vibration Reduction in Turning. Journal of Metallic Material Research| Volume, 2023, 6(01). https://doi.org/10.30564/jmmr.v6i1.5428

[38] Keränen, L., M. Pylvänäinen, A. Kaijalainen, T. Jokiaho, et al., Residual stresses of MAG-welded ultrahigh-strength steel rectangular hollow sections. Engineering Structures, 2024, 305: p. 117719. https://doi.org/10.1016/j.engstruct.2024.117719

[39] Güven, F. and H. Rende, An analysis of endurance limit-modifying factors depending on bead shape and thickness in load-carrying welded T-joints. Journal of the Brazilian Society of Mechanical Sciences and Engineering, 2020, 42: p. 1-8. https://doi.org/10.1007/s40430-020-2171-3

[40] Schwarz, B.J. and M.H. Richardson, Experimental modal analysis, in CSI Reliability week. 1999. p. 1-12.

[41] Greenspon, J.E., Acoustics, linear. 2003. p. 129-167. https://doi.org/10.1016/B0-12-227410-5/00009-0

[42] Sun, J., T. Nitschke-Pagel, and K. Dilger, Influence of temperature-and phase-dependent yield strength on residual stresses in ultra-high strength steel S960 weldments. journal of materials research and technology, 2021, 15: p. 1854-1872. https://doi.org/10.1016/j.jmrt.2021.09.050

[43] Heinze, C., C. Schwenk, and M. Rethmeier, Numerical calculation of residual stress development of multi-pass gas metal arc welding. Journal of Constructional Steel Research, 2012, 72: p. 12-19. https://doi.org/10.1016/j.jcsr.2011.08.011

[44] Ewins, D., Modal Testing: Theory and Practice, Research Studies Press. 1984, England.

[45] Khot, S. and N.P. Yelve, Modeling and response analysis of dynamic systems by using ANSYS© and MATLAB©. Journal of Vibration and Control, 2011, 17(6): p. 953-958. https://doi.org/10.1177/1077546310377913

[46] Pei, X., S.K. Ravi, P. Dong, X. Li, and X. Zhou, A multi-axial vibration fatigue evaluation procedure for welded structures in frequency domain. Mechanical Systems and Signal Processing, 2022, 167: p. 108516. https://doi.org/10.1016/j.ymssp.2021.108516

Submitted: 01.3.2024
Accepted: 02.6.2025

Osman Bahadır Özden*
MPG Machinery Production Group Inc. Co., Turkey
Barış Gökçe
Department of Mechatronics Engineering, Necmettin Erbakan University, Turkey
Abdullah Erdemir
MPG Machinery Production Group Inc. Co., Turkey
*Corresponding Author: bozden@mpg.com.tr